

Detailed analysis of the variable star population in the globular cluster NGC 7006.

A. Arellano Ferro,^{1*} F. C. Rojas Galindo,^{1†} I. H. Bustos Fierro,² S. Muneer³

M.A. Yepez,¹ Sunetra Giridhar³

¹*Instituto de Astronomía, Universidad Nacional Autónoma de México, Ciudad Universitaria, C.P. 04510, México*

²*Observatorio Astronómico, Universidad Nacional de Córdoba, Córdoba C.P. 5000, Argentina*

³*Indian Institute of Astrophysics, Sarjapur Main Road, 2nd Block, Koramangala 560034, Bangalore, India*

Accepted XXX. Received YYY; in original form ZZZ

ABSTRACT

A five year CCD photometric *VI* time-series of NGC 7006 is employed to perform a detailed analysis of the known population of variable stars. In the process we have corrected inconsistent classifications, sky coordinates and found ten new cluster member variables. An independent reddening estimate with a value $E(B - V) = 0.08 \pm 0.05$ is made. Using Fourier decompositions of RR Lyrae light curves and well established calibrations, the cluster mean metallicity and distance $[\text{Fe}/\text{H}]_{\text{ZW}} = -1.53 \pm 0.15$ and 41.2 ± 1.4 kpc are estimated based on an extended sample of cluster member RRab stars. Using the *Gaia*-DR3 data we performed an extensive membership analysis which leads to a clean Colour-Magnitude diagram, and hence to the identification of variables that are likely field stars, and to considerations on the variables distribution in the Horizontal Branch (HB). A double mode RR Lyrae and three CW star are discussed. The origin of CW stars from precursors in the blue tail of the HB with very thin ($\sim 0.06 \pm 0.01 M_{\odot}$) envelopes is argued. Our models indicate that the Main Sequence predecessor of RR Lyrae stars had a mass of $0.82\text{--}0.85 M_{\odot}$ and lost about 25-35% of its mass during the red giant branch events before settling in the HB some 12-13.5 Gyrs later.

Key words: variable stars – RR Lyrae – fundamental parameters – globular cluster – NGC 7006

1 INTRODUCTION

The study of the variable star populations in globular clusters from CCD time-series imaging has proven to be successful in the determination of physical parameters such as the metallicity and distance, and in the detailed description of the Color Magnitude diagram structure. The approach has also enabled us to complete the variable star population census of the cluster under study, to improve upon the pulsation periods and to correct variable star type classifications, to confirm the variable vs non-variable nature of many misclassified stars and often to correct sky coordinates and to accurately identify all variables star in the field of the cluster. Furthermore, the recent publication of the results of the *Gaia* mission, the DR3 release, and the development of powerful statistical numerical approaches, offer an unprecedented opportunity to separate the cluster members from the field stars, which leads to more accurate Colour-Magnitude diagrams (CMD), and particularly the distribution of member variables stars and their confrontation with their evolutionary properties. For all the above reasons there is a renewed

interest in depth study of dense time series of images of globular clusters.

The present work, focused on the globular cluster NGC 7006, is part of the long effort to employ the RR Lyrae stars light curves as indicators of their physical parameters, via the Fourier decomposition. A recent summary of the results for 35 globular clusters can be found in paper by [Arellano Ferro \(2022\)](#). In that work the author argues in favour of the accuracy of the metallicities and distances rendered by the approach.

NGC 7006 is located in the constellation Delphinus ($\alpha = 21^{\text{h}}01^{\text{m}}29.38^{\text{s}}$, $\delta = +16^{\circ}11'14.4''$, J2000). Its present galactic position is $l = 63.77^{\circ}$, $b = -19.41^{\circ}$ and $Z = -13.7$ kpc, although its long-term orbit show diversions as large as $|Z| = 56.13$ kpc ([Allen et al. 2006](#)). It is a cluster rich in RR Lyrae stars, 64 of them are recorded in the Catalogue of Variable Stars in Globular Clusters ([Clement et al. 2001](#)). The only other type of variables known in the cluster before the present work were two red giant star of the types SR8 (V19) and L (V54). A comprehensive study of the 76 variables presently known in NGC 7006 and their periods was published by [Wehlau et al. \(1999\)](#) (hereinafter WSN99).

In this paper we report the results of a time-series *VI* CCD photometry of the variable stars in the field of the cluster, discuss the stellar cluster membership, estimate relevant phys-

* E-mail: armando@astro.unam.mx

† E-mail: fcrojas@astro.unam.mx

Table 1. The distribution of observation of NGC 7006^a.

Date	N _V	t _V (s)	N _I	t _I (s)	Mean seeing (″)
2011/10/05	8	120-300	10	20-80	2.0
2011/10/06	7	100	8	40	1.9
2012/08/23	9	60-240	0	-	1.8
2012/08/25	55	60-240	0	-	1.8
2013/07/30	2	110-120	5	40-50	1.6
2013/07/31	22	105-110	26	40-55	1.9
2013/08/01	31	75-120	31	35-60	1.7
2013/08/26	28	100-110	27	50-60	1.7
2013/08/27	25	60-90	28	35-50	1.6
2015/06/26	4	300	6	130	2.0
2015/06/27	8	300	8	130	1.9
Total:	199		149		

^aColumns N_V and N_I indicate the number of images obtained in the V-band and I-band, respectively. Columns t_V and t_I are the range of exposure time used during each night. In the last column, the mean seeing in arc seconds for each night are listed.

ical parameters of RR Lyrae stars via the Fourier decomposition of their light curves, particularly the cluster mean metallicity and distance, discuss the horizontal branch (HB) structure, and the time scales and mass of the precursor main sequences stars of the present RR Lyrae. We also performed a routinely search of previously undetected variables and report the discovery of ten new variables; two RRab, two RRc, one CWB (or BL Her) star and five semi regular or SR stars (see §4.1). We discuss the non cluster member status of several variables and have noticed the need to correct a few variable types. Notes on individual stars are to be found in Appendix A.

2 OBSERVATIONS AND REDUCTIONS

CCD VI image of NGC 7006 were obtained during 11 nights over 4 years: 2011 October 5-6, 2012 August 23-25, 2013 between July 30 and August 27, and 2015 June 26-27. The observations were performed with the 2 m telescope at the Indian Astronomical Observatory (IAO) in Hanle, India. The detector used was a SITe ST-002 2Kx4K CCD pixels with a scale of 0.296 arcsec/pix, translating to a field of view (FoV) of approximately 10.1×10.1 arcmin².

Table 1 contains the log of the observations and includes the date, number of images and exposure time by filter and the mean seeing nightly conditions.

2.1 Difference image analysis

All cluster frames were corrected via numerous bias and sky flat field images through standard procedures. For the extraction of accurate photometry, we employed the difference image analysis (DIA) technique, for which the DanDIA pipeline was used (Bramich 2008; Bramich et al. 2013). This approach has been repeatedly used and described in detail in previous publications. The interested reader can find a thorough description of the approach and the conversion of fluxes into magnitudes in the paper by Bramich et al. (2011).

Table 2. Time-series VI photometry for the variables stars observed in this work^a.

Variable Star ID	Filter	HJD (d)	M _{std} (mag)	m _{ins} (mag)	σ _m (mag)
V1	V	2455840.08949	19.201	20.286	0.022
V1	V	2455840.09717	19.232	20.317	0.025
⋮	⋮	⋮	⋮	⋮	⋮
V1	I	2455840.06083	18.479	19.785	0.055
V1	I	2455840.08418	18.536	19.842	0.031
⋮	⋮	⋮	⋮	⋮	⋮
V2	V	2455840.08949	19.157	20.239	0.020
V2	V	2455840.09717	19.168	20.250	0.022
⋮	⋮	⋮	⋮	⋮	⋮
V2	I	2455840.06083	18.386	19.690	0.049
V2	I	2455840.08418	18.451	19.755	0.027
⋮	⋮	⋮	⋮	⋮	⋮

^aThe variable star, filter used and epoch of mid-exposure are listed in columns 1, 2 and 3, respectively. The instrumental magnitudes, m_{ins}, and standard magnitudes, m_{std}, corresponding to each variable star are listed in the columns 4 and 5, in addition, the column 6 contains the uncertainty of the instrumental magnitude, σ_m, which also corresponds to the error of the standard magnitude. The full version of this table is available at the CDS data base.

2.2 Transformation to the standard system

The transformation of the instrumental *vi* magnitudes to the standard VI Johnson–Kron–Cousins standard system (Landolt 1992), was performed using about 300 standard stars in the FoV of NGC 7006 included in the catalogue of standard stars in globular clusters of (Stetson 2000). Linear fits to the correlations (*v* − *i*) vs. (*V* − *v*) and (*v* − *i*) vs. (*I* − *i*), carry a small colour dependence, as is generally expected. The transformation equations are form:

$$V - v = +0.044(\pm 0.004)(v - i) - 1.096(\pm 0.004), \quad (1)$$

$$I - i = +0.031(\pm 0.004)(v - i) - 1.314(\pm 0.004), \quad (2)$$

In Table 2, we show a small fragment of the resulting time-series VI photometry for each variable star obtained in this work. The full table shall be available in electronic form in the *Centre de Données astronomique de Strasbourg* data base (CDS).

3 STAR MEMBERSHIP IN THE FOV OF NGC 7006

To establish the membership status of the stars in our FoV, we have employed the high-quality astrometric data available in *Gaia*-DR3 (Gaia Collaboration et al. 2021) and the method developed by Bustos Fierro & Calderón (2019), which consists of two main stages:

- The first stage is based on a clustering algorithm applied

to a multidimensional space of physical parameters. It aims to find groups of stars that possess similar characteristics in the four-dimensional space of the gnomonic coordinates (X_t, Y_t) and proper motions ($\mu_{\alpha*}, \mu_{\delta}$).

- The second stage consists of the analysis of the projected distribution of stars with different proper motions around of the mean proper motion of the cluster, and it is aimed to identify probable missing members.

The method was applied to 3316 Gaia-sources in a field of radius 10 arcmin centered in the cluster, of which 530 were identified as likely cluster members. Fig. 1 displays the Vector Point Diagram (VPD), where the distribution of the proper motions is shown, and the resulting Color-Magnitude diagram (CMD) of likely cluster members.

We were able to measure light curves for 1373 stars in the FoV of our images, 470 of which are among the likely cluster members, enabling to refine the working CMD that shall be discussed later in the paper.

4 VARIABLE STARS IN NGC 7006

4.1 Search for new variables

Taking advantage of the resulting time-series VI for the 470 stars likely to be cluster members in our FoV, we performed a routine search for new variables. For this purpose we splitted the CMD of NGC 7006 into regions where variable stars are typically found. We selected four regions: the Blue Stragglers (BS), the Horizontal Branch (HB), the W Virginis and BL Herculis region above of the HB, and the Tip of the Red Giant Branch (TRGB). We analyzed the light curves of the stars belonging to these regions, and calculated their period using the string-length method (Burke et al. 1970; Dworetsky 1983), and phase their light curves. With this method we discovered 10 new variables and have assigned them variable numbers as follows: two RRc (V77 and V78), two RRab stars (V79 and V80), one BL Hercules star (V81) and five SR stars (V82, V83, V84, V85 and V86). Their folded light curves are shown in Fig. 3.

Gerashchenko (2006) had suggested the existence of two new variable stars which he called V77 and V78, however we identified these stars in our photometry collection and found them not to be variable. These stars are not registered in the CVSGC, so we do not take them into account when naming the stars discovered in this work.

Table 3 lists all the variable stars presently known in NGC 7006 and shows the basic photometric and positional data and membership status for each variable. The reported periods found in our data are listed in column 7, while in column 8 we include the periods reported by WSN99. With a few exceptions the periods are very similar. All variable stars listed in Table 3 have been identified in the charts of Fig. 2.

4.2 The RR Lyrae stars

4.2.1 RR Lyrae variable stars in NGC 7006

During the analysis we noticed that several stars had a wrong classification or coordinates slightly off the position of the corresponding variable both in our astrometrically calibrated

image and in the *GAIA*-DR3 release. The corrected types and coordinates are those listed in Table 3.

The total number of RR Lyrae stars in Table 3 is 71 but a few stars were considered field stars, as indicated in the last column of this table. There are 49 RRab, 7 RRc, 1 RRd likely cluster members. Furthermore, we noticed that the RRab stars V3, V12, V16 and V63 show Blazhko-like amplitude modulations not previously reported. Please refer to Appendix A for details on individual stars.

4.2.2 Oosterhoff type

The average period of the RRab stars in NGC 7006 is $\langle P_{ab} \rangle = 0.577 \pm 0.006$ d, the estimated uncertainty is the standard error of the mean, and the fraction of RRc stars is $N_c/(N_c + N_{ab}) = 0.14$. These values clearly identify NGC 7006 as a Oosterhoff type OoI, consistent with the classification made by Gerashchenko & Ananjevskaja (2018).

Furthermore, the period-amplitude plane for RR Lyrae stars, also known as the Bailey diagram shown in Fig. 4 for the V and I light curve amplitudes, also confirm the OoI type of the cluster. The amplitudes were estimated from the best fit obtained by the Fourier decomposition of the light curves. For the stars with Blazhko-like modulations, the maximum amplitude was taken. The distribution of RRab stars and the reference loci for unevolved and evolved stars (OoI and OoII), described in the figure caption, clearly confirm the cluster as of the OoI type. The anomalous position of the some stars in the Bailey diagram will be discussed in Appendix A.

4.2.3 Reddening estimate from RRab stars

Sturch (1966), demonstrated that in RRab stars the minimum colour between phases 0.5 and 0.8, $(V - I)_{min}$, is constant. Guldenschuh et al. (2005) calibrated the intrinsic color between the same phases as $(V - I)_{0,min} = 0.58 \pm 0.02$. Using these results, reddening $E(V - I)$ can be estimated. We obtained the value of $E(B - V)$ from the ratio $E(V - I)/E(B - V) = 1.259$ (e.g. Yepez et al. 2020). Employing 41 RRab stars whose light curves were of best quality we obtained an average reddening $E(B - V) = 0.08 \pm 0.05$. The large uncertainty is mainly due to the noise in our light curves.

It is of interest to recall the values of interstellar reddening estimated from the position of the cluster by Schlafly & Finkbeiner (2011), $E(B - V)_{S\&F} = 0.07 \pm 0.003$, and Schlegel et al. (1998) (SFD), $E(B - V)_{SFD} = 0.08 \pm 0.004$. Henceforth we shall adopt $E(B - V) = 0.08$ for the rest of the present work.

4.3 Other variable stars

While the variable star population of NGC 7006 is dominated by the presence of RR Lyrae stars, luminous variables near the TRGB are also present: seven SR type (V19, V70, V82, V83, V84, V85 and V86), one L type (V54) and one that we could not classify (V34). Their light curves are shown in figure 3 phased with the periods listed in Table 3 which are accurate only to the second digit.

Table 3. Data of variable stars in NGC 7006 in the FoV of our images.

Variable Star ID	Variable Type	$\langle V \rangle$ (mag)	$\langle I \rangle$ (mag)	A_V (mag)	A_I (mag)	$P(d)$ This work	$P(d)$ WSN99	HJD _{max} (+2450000)	RA (J2000.0)	Dec (J2000.0)	Mem ^b
V1	RRab	18.901	18.389	1.121	0.794	0.492730	0.492731	6531.1366	21:01:16.81	+16:13:07.1	Y
V2	RRab	18.916	18.329	0.961	0.578	0.586961	0.586984	6505.3307	21:01:26.73	+16:10:34.9	Y
V3	RRab Bl	18.943	18.292	0.806	0.420	0.559646	0.560555	6163.2429	21:01:27.48	+16:11:46.2	Y
V5	RRab	18.839	18.291	0.832	0.607	0.535095	0.533288	6532.2167	21:01:27.74	+16:11:50.4	Y
V6	RRab	19.005	18.427	1.109	0.704	0.498056	0.498032	6532.1130	21:01:28.23	+16:10:27.6	Y
V8	RRab	19.097	18.384	0.913	0.651	0.564299	0.564293	6165.2675	21:01:31.58	+16:11:25.6	Y
V10	RRab	18.942	18.387	0.920	0.694	0.542048	0.542908	7201.3771	21:01:32.15	+16:11:00.3	Y
V11	RRab	18.958	18.322	0.864	0.505	0.576019	0.576032	6532.1296	21:01:39.53	+16:12:02.4	Y
V12	RRab Bl	18.902	18.259	0.755	0.441	0.574076	0.576032	6532.1678	21:01:37.64	+16:10:08.0	Y
V13	RRab	18.953	18.364	0.990	0.667	0.551647	0.551646	6531.1366	21:01:36.31	+16:11:51.7	Y
V14	RRab	18.958	18.327	0.917	0.641	0.560362	0.560360	6506.4312	21:01:31.65	+16:13:20.1	Y
V15	RRab	18.883	18.239	0.852	0.599	0.588070	0.588070	6506.3946	21:01:28.41	+16:13:06.5	Y
V16	RRab Bl	18.858	18.214	1.170	0.789	0.537565	0.537576	6532.1760	21:01:26.47	+16:13:27.2	Y
V17	RRab	18.934	18.389	1.104	0.869	0.511497	0.511497	6506.4556	21:01:22.28	+16:12:31.9	Y
V18	RRab Bl	18.955	18.314	0.764	0.551	0.603724	0.603707	6505.2748	21:01:27.13	+16:09:42.6	Y
V19	SR	15.601	14.047	-	-	41.0	92.17	6504.4353	21:01:29.18	+16:10:46.7	Y
V20	RRab	18.961	18.381	0.861	0.643	0.577536	0.577533	6165.3221	21:01:27.73	+16:10:47.7	Y
V21	RRab	18.910	18.236	0.786	0.459	0.612548	0.612559	6165.3559	21:01:27.72	+16:10:53.8	Y
V22	RRab	18.935	18.367	1.048	0.633	0.526925	0.526925	6165.2536	21:01:28.31	+16:10:56.4	Y
V23	RRab	18.797	18.193	0.876	0.561	0.606899	0.607949	6163.2429	21:01:27.29	+16:11:04.4	Y
V24	RRab	18.356	17.918	0.396	0.301	0.609384	0.627156	6163.2513	21:01:27.40	+16:11:09.1	N
V25	RRab Bl	18.844	18.392	0.913	0.735	0.543231	0.543232	6532.1678	21:01:27.83	+16:11:17.1	Y
V26	RRab	18.628 ^a	-	0.9 ^a	-	-	0.540697	-	21:01:28.44 ^a	+16:11:08.6 ^a	?
V27	RRab	18.257	17.737	0.582	0.371	0.564680	0.564124	6504.4440	21:01:28.38	+16:11:12.3	N
V28	RRd?	19.012	18.465	1.191	0.748	0.33213	0.496958	6531.2216	21:01:28.13	+16:11:17.9	Y
V29	RRab	18.975	18.350	0.976	0.717	0.559245	0.559197	6504.4353	21:01:31.6	+16:11:43.4	Y
V30	RRab	18.634	18.221	0.661	0.571	0.568951	-	6506.3704	21:01:29.56	+16:11:28.8	?
V31	RRab	18.901	18.092	0.966	0.497	0.563464	0.563139	6532.1110	21:01:29.88	+16:11:23.3	Y
V32	RRab	18.756	18.214	0.733	0.503	0.562648	0.562653	6506.3921	21:01:30.65	+16:11:26.0	Y
V33	RRab	19.032	18.348	0.997	0.625	0.556801	0.556807	6532.1296	21:01:31.39	+16:11:34.5	Y
V34	EW?	17.884	16.744	-	-	0.908797	-	6163.2557	21:01:30.89	+16:11:15.5	Y
V35	RRab	18.983	18.313	0.727	0.564	0.596268	0.596265	6163.2578	21:01:31.70	+16:11:09.7	Y
V36	RRc	-	-	-	-	-	0.276970	-	21:01:30.94 ^a	+16:11:07.6 ^a	?
V37	RRab	-	-	-	-	-	0.5679 ^d	-	21:01:30.50 ^a	+16:11:08.1 ^a	Y
V38	RRab	18.837	18.282	0.830	0.644	0.622316	0.624434	6531.2191	21:01:30.68	+16:10:53.6	Y
V39	RRab	-	-	-	-	-	0.578450	-	21:01:29.99 ^a	+16:10:46.4 ^a	Y
V41	RRab	18.635	17.914	0.762	0.427	0.566347	0.566852	6165.3736	21:01:29.30	+16:11:00.8	N
V42	RRab	18.458	17.941	-	-	0.746606	-	6165.3559	21:01:29.86	+16:11:04.4	N
V43	RRab	18.944	18.330	0.622	0.471	0.596600	0.596614	6531.2216	21:01:28.93	+16:10:43.4	Y
V44	RRab	18.910	18.285	0.727	0.481	0.587795	0.587779	6506.2512	21:01:38.90	+16:08:18.1	Y
V45	RRab	18.903	18.229	0.752	0.504	0.583846	0.583852	6531.2897	21:01:15.95	+16:09:55.7	Y
V46	RRab	18.872	18.272	0.318	0.234	0.668906	0.667587	6532.1130	21:01:20.51	+16:10:16.3	Y
V47	RRab	18.949	18.343	0.653	0.515	0.567464	0.568285	6532.1739	21:01:16.41	+16:10:48.3	Y
V48	RRab	18.967	18.304	0.718	0.522	0.611972	0.611975	6506.4556	21:01:22.33	+16:12:43.7	Y
V49	RRab	18.984	18.355	0.859	0.434	0.581855	0.581895	6506.3489	21:01:29.78	+16:11:53.8	Y
V50	RRab	18.919	18.317	0.835	0.630	0.590330	0.590383	6505.4599	21:01:26.37	+16:11:04.9	Y
V51	RRab	18.977	18.254	0.439	0.315	0.643829	0.643838	6505.4599	21:01:33.26	+16:11:59.1	Y
V52	RRab	18.938	18.246	0.550	0.465	0.621717	0.621703	6506.2459	21:01:29.36	+16:12:38.7	Y
V53	RRc	18.837	18.500	0.248	0.230	0.260171	0.357694	6165.2674	21:01:32.56	+16:11:03.2	Y
V54	L	16.081	14.778	-	-	30.7	-	6163.2513	21:01:29.46	+16:10:42.4	Y
V55	RRab	-	-	-	-	-	0.537738	-	21:01:12.40 ^a	+16:16:13.9 ^a	?
V56	RRab	19.086	18.365	1.097	0.713	0.547423	0.549655	6531.1929	21:01:28.45	+16:10:59.9	Y
V57	RRc	18.956	18.518	0.630	0.407	0.351903	0.351893	6532.1657	21:01:28.76	+16:10:59.9	Y
V58	RRab	18.851	18.157	0.256	0.213	0.743666	0.5150 ^d	6532.1110	21:01:30.27	+16:11:28.2	Y
V59	RRab	18.975	18.463	1.093	0.830	0.480997	0.480985	5841.0670	21:01:31.01	+16:11:21.0	Y
V60	RRab	18.913	18.189	0.611	0.385	0.626593	0.385810	6506.3704	21:01:28.46	+16:11:19.7	Y
V61	RRab	18.816	18.284	1.025	0.645	0.589081	0.589097	6506.2858	21:01:26.66	+16:11:32.1	N
V62	RRc	18.873	18.349	0.439	0.322	0.346931	0.346946	6532.1981	21:01:27.70	+16:11:15.5	Y
V63	RRab Bl	18.800	18.296	0.957	0.699	0.547209	0.5280 ^d	5840.1197	21:01:30.22	+16:11:33.8	Y

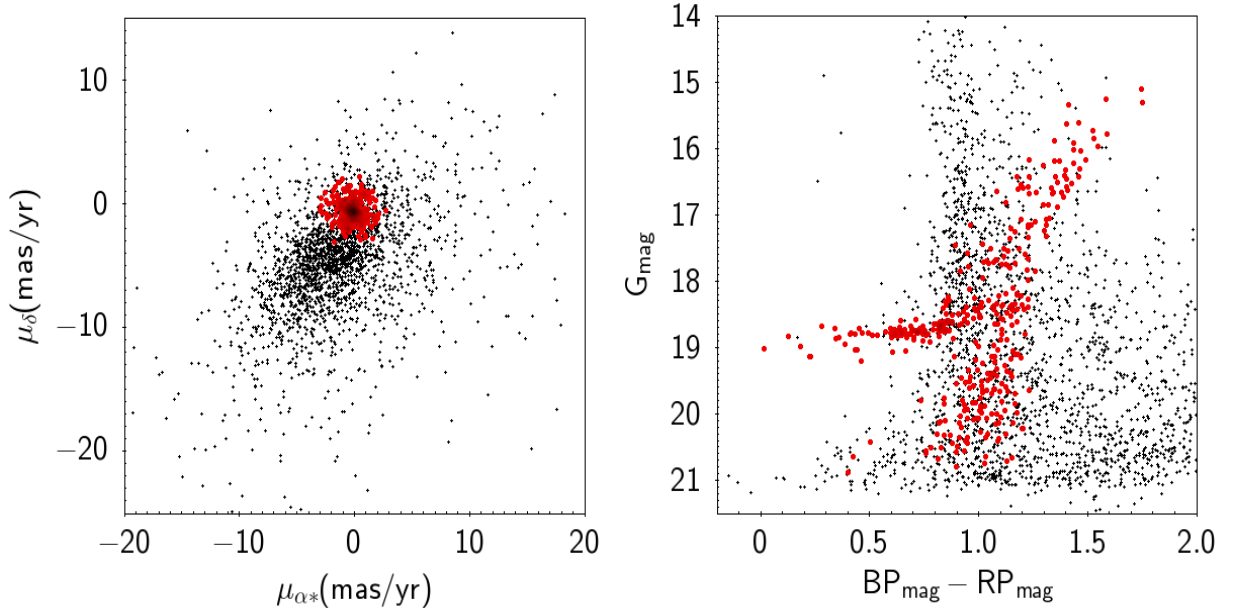


Figure 1. Red and gray points correspond to the stars that were found cluster members and non-members, respectively. Left-hand panel: VPD of the cluster NGC 7006; right-hand panel: color-magnitude diagram of NGC 7006 in the Gaia's photometric system.

Table 3. Continued

Variable Star ID	Variable Type	$\langle V \rangle$ (mag)	$\langle I \rangle$ (mag)	A_V (mag)	A_I (mag)	P (d) This work	P (d) WSN99	HJD _{max} (+2450000)	RA (J2000.0)	Dec (J2000.0)	Mem ^b
V64	RRc	18.877	18.528	0.386	0.296	0.306375	0.313142	6504.4353	21:01:30.68	+16:11:17.5	Y
V65	RRab	18.776	18.220	0.563	0.456	0.558761	-	6165.3559	21:01:28.63	+16:11:22.2	Y
V66	RRc	18.452	17.628	0.339	0.141	0.361055	0.6172 ^d	6506.3161	21:01:31.09	+16:11:08.5	Y
V67	RRab	18.508	17.699	0.408	0.213	0.554945	0.3175 ^d	6504.4440	21:01:28.21	+16:11:11.3	N
V68	RRab	19.015	18.323	0.995	0.641	0.555726	-	6506.3562	21:01:30.18	+16:11:16.9	Y
V69	RRab	19.422	18.615	1.466	0.727	0.656633	-	5841.0670	21:01:29.89	+16:11:15.7	N
V70	CW	16.680	15.570	-	-	11.7	-	6165.3559	21:01:29.81	+16:11:12.4	Y
V71	RRc	18.703	18.198	0.494	0.306	0.335231	0.348346	6165.3559	21:01:28.99	+16:10:58.3	N
V72	RRc	-	-	-	-	-	-	-	21:01:30.96 ^a	+16:11:09.8 ^a	?
V73	RRab	18.129	17.276	0.566	0.341	0.554953	0.5780 ^d	6165.3580	21:01:28.18	+16:11:12.7	N
V74	= V41										
V75	CWA	18.628	17.917	0.121	0.086	13.5071	-	6506.4556	21:01:39.30	+16:08:29.9	N
V76	RRab	19.118	18.195	1.240	0.598	0.566262	0.56170	6532.1657	21:01:29.84	+16:11:24.8	Y?
V77 ^c	RRc	19.044	18.252	0.086	0.074	0.317159	-	6165.3600	21:01:24.24	+16:11:52.7	Y
V78 ^c	RRc	18.805	18.176	0.261	0.174	0.332177	-	6505.3514	21:01:28.26	+16:11:18.0	Y
V79 ^c	RRab	19.055	18.363	0.804	0.653	0.598871	-	6531.3100	21:01:28.68	+16:11:03.0	Y
V80 ^c	RRab	19.181	18.809	0.119	0.098	0.541755	-	6165.2563	21:01:29.43	+16:10:56.9	Y
V81 ^c	CWB	17.888	17.185	-	-	4.63	-	6165.3559	21:01:29.44	+16:11:15.6	Y
V82 ^c	SR	16.455	15.131	-	-	14.01	-	6504.4440	21:01:26.78	+16:11:30.6	Y
V83 ^c	SR	15.934	14.278	-	-	18.68	-	6532.1110	21:01:29.77	+16:11:15.1	Y
V84 ^c	SR	16.266	14.940	-	-	10.22	-	6165.3538	21:01:29.98	+16:11:02.9	Y
V85 ^c	SR	15.858	14.262	-	-	8.37	-	6165.3642	21:01:30.80	+16:11:23.9	Y
V86 ^c	SR	16.215	14.775	-	-	36.14	-	6532.1110	21:01:31.33	+16:11:13.9	Y

Bl: RR Lyrae with Blazhko effect. Amplitudes for this star correspond to the maximum observed.

^a Value taken from CVSGC (Clement et al. 2001).

^b Membership status: Y = member, N = no-member, ? no proper motions available, or dubious membership.

^c New variable star found in this work.

^d Period from Pinto & Rosino (1973)

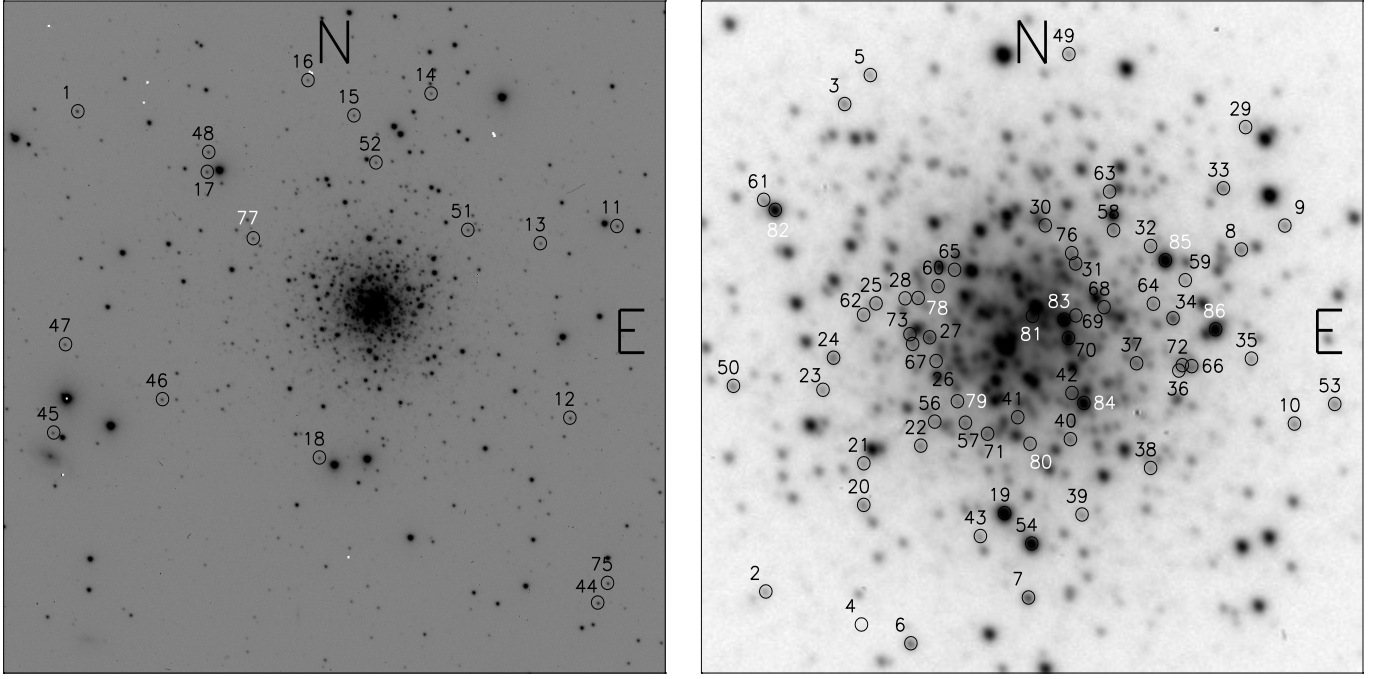


Figure 2. Identification charts of all variable stars in NGC 7006 listed in Table 3. The panels are constructed from the V reference image, built by stacking the best quality images in our collection. The left panel shows a field of 6.7×6.7 arcmin². The panel to the right displays the central region of the cluster with a field of 1.63×1.63 arcmin². The labels refer to the variable numbers and those labeled in white are newly discovered in this work.

5 PHYSICAL PARAMETERS OF RR LYRAE STARS

The light-curve morphology of RR Lyrae stars is tightly related to some of fundamental physical parameters of the star and of the cluster to which they belong, of particular relevance being the metallicity or $[\text{Fe}/\text{H}]$ and the distance. The Fourier decomposition of the light curve in harmonics, is parameterized by an equation of the form

$$m(t) = A_0 + \sum_{k=1}^N A_k \cos\left(\frac{2\pi k}{P}(t - E) + \phi_k\right), \quad (3)$$

where $m(t)$ is the magnitude at time t , P is the period in days, E is the epoch or time of maximum light and N is the degree or number of harmonics used to reproduce the curve. A_0 is the intensity weighted mean, that is the best estimation of mean magnitude of the light curve. We used a linear minimization routine to derive the best fit values of the amplitude A_k and phase ϕ_k of each harmonic and from which we can calculate the Fourier parameters defined as $\phi_{ij} = j\phi_i - i\phi_j$ and $R_{ij} = A_i/A_j$, with $1 \leq i, j \leq N$.

This approach to the calculation of the mean metallicity and distance of globular clusters with RR Lyrae stars has proven to be very accurate and the results compare very well, within the respective uncertainties with spectroscopic $[\text{Fe}/\text{H}]$ values and distances obtained via Gaia-DR3 and HST, as it has been recently discussed by Arellano Ferro (2022) for a sample of 37 globular clusters.

The calibrations that correlate the Fourier and the physical parameters for RRab and RRc stars and their zero points, have been described in detail by Arellano Ferro (2022) and in

many of the references cited there, hence we will not repeat them here. The calibrations and their zero points can also be found summarized in Table 4 of Yezpez et al. (2022). We should recall however, that the $[\text{Fe}/\text{H}]$ calibration for RRab stars (Jurcsik & Kovacs 1996), is valid only for stars with a defined consistency parameter $D_m < 3.0$. In order to include a more solid sample we have slightly relaxed this condition and we have taken stars with $D_m < 5.0$.

In Table 4 we provide the Fourier coefficients of all stars measured by our photometry, however, not all the stars were considered for the physical parameters calculation due to several reasons; first, if $D_m > 5.0$, or if the star position on the CMD is noticeable peculiar mostly due to unresolved blends, or if the membership analysis and the resulting distance suggest that the star is a field star. The peculiarities of individual stars are presented in Appendix A.

In Table 5 we list the resulting physical parameters only for stars with consistent light curves and likely cluster members.

5.1 The mean metallicity and distance

Columns 2 and 3 of Table 5 contain the iron abundance value in the scale of Zinn & West (1984) $[\text{Fe}/\text{H}]_{\text{ZW}}$ and its transformation to the *Ultraviolet and Visual Echelle Spectrograph* (UVES) scale of Carretta et al. (2009) $[\text{Fe}/\text{H}]_{\text{UVES}}$ respectively, correlated via the equation,

$$[\text{Fe}/\text{H}]_{\text{UVES}} = -0.413 + 0.130[\text{Fe}/\text{H}]_{\text{ZW}} - 0.356[\text{Fe}/\text{H}]_{\text{ZW}}^2. \quad (4)$$

For completeness, column 4 of Table 3 lists the value given

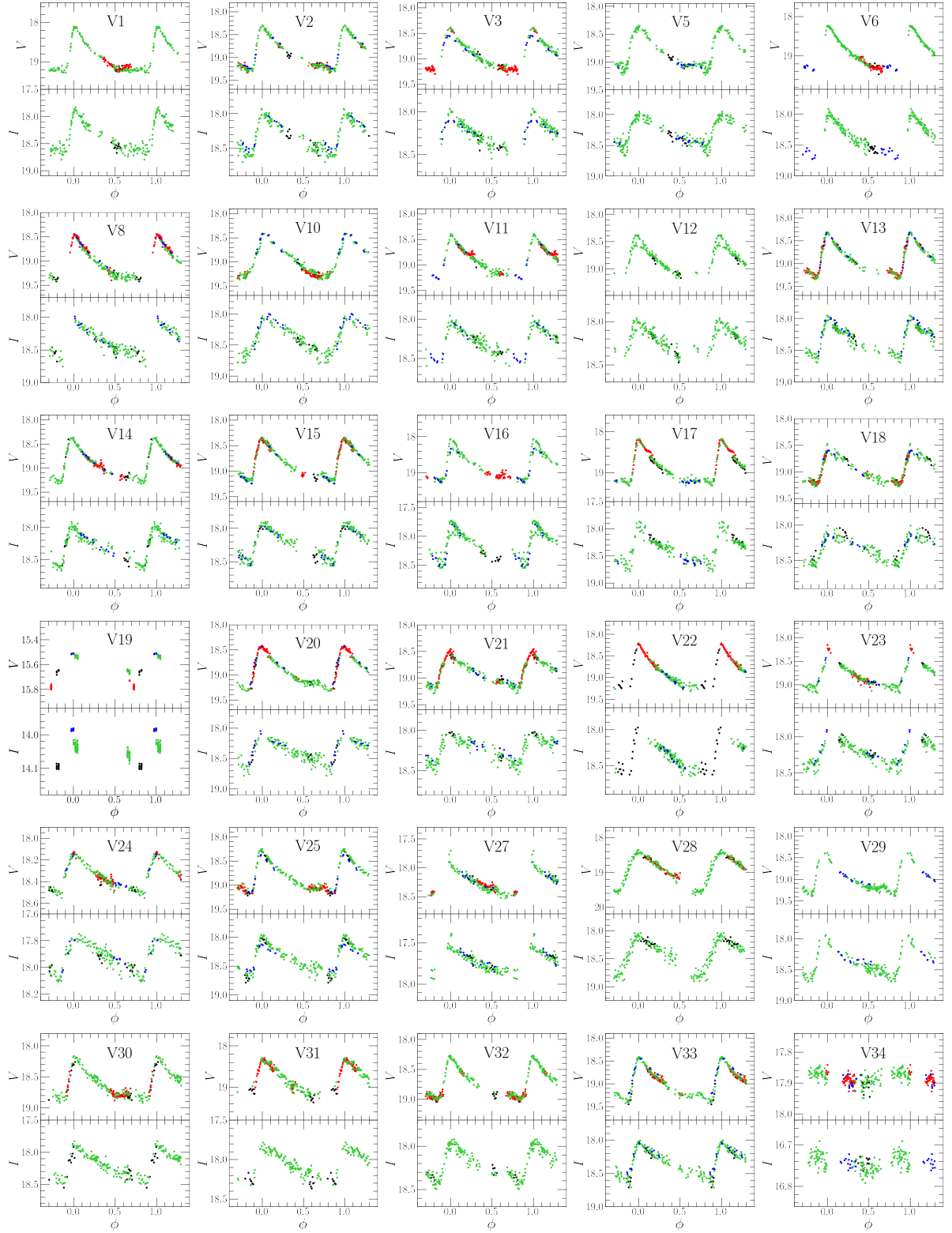


Figure 3. Light curves of 75 variable in the field of view of NGC 7006. For membership conclusions refer to the last column of Table 3. All light curves are phased with the ephemerides given in that table. V75 is plotted as function of HJD to highlight its long-term variation. For a phased light curve and a discussion of this star please refer to Appendix A. In this mosaic the symbols colours are coded as: black, red, green and blue for the 2011, 2012, 2013 and 2015 seasons.

Table 4. Fourier coefficients of the V light curves of RRab and RRC stars in NGC 7006. The deviation parameter D_m is also listed for the RRab stars.

Variable ID	A_0 (V mag)	A_1 (V mag)	A_2 (V mag)	A_3 (V mag)	A_4 (V mag)	ϕ_{21}	ϕ_{31}	ϕ_{41}	D_m
RRab									
V1	18.901(4)	0.406(5)	0.182(5)	0.146(5)	0.076(5)	3.793(39)	7.932(53)	5.585(85)	4.9
V2	18.916(4)	0.332(6)	0.176(6)	0.107(5)	0.088(6)	4.194(46)	8.250(74)	6.684(93)	5.7
V3	18.943(4)	0.317(5)	0.143(5)	0.095(5)	0.056(5)	4.047(52)	8.303(72)	6.109(112)	3.3
V5	18.839(5)	0.303(7)	0.128(7)	0.091(8)	0.048(7)	3.905(75)	8.031(103)	6.307(178)	2.6
V6	19.005(5)	0.413(8)	0.183(7)	0.142(6)	0.087(6)	3.886(54)	7.905(76)	6.002(112)	6.2
V8	19.097(4)	0.341(5)	0.162(6)	0.122(5)	0.068(5)	3.848(47)	8.103(67)	6.093(106)	1.9
V10	18.942(5)	0.385(7)	0.125(6)	0.071(7)	0.026(5)	4.416(62)	8.487(96)	6.322(287)	6.0
V11	18.958(3)	0.299(5)	0.130(5)	0.104(5)	0.064(5)	3.888(51)	8.263(70)	6.215(100)	5.3
V12	18.958(3)	0.286(5)	0.126(7)	0.095(6)	0.049(6)	3.649(72)	7.778(102)	5.536(162)	2.0
V13	18.953(5)	0.324(7)	0.159(7)	0.113(7)	0.082(7)	3.757(60)	7.997(83)	5.815(117)	2.7
V14	18.958(4)	0.314(6)	0.153(7)	0.113(7)	0.072(6)	3.986(43)	8.162(64)	6.128(103)	3.1
V15	18.883(3)	0.300(5)	0.139(5)	0.094(4)	0.066(4)	3.907(46)	8.137(72)	6.222(98)	3.9
V16	18.858(7)	0.369(10)	0.197(9)	0.150(10)	0.099(10)	3.885(70)	8.186(99)	5.899(141)	4.3
V17	18.934(4)	0.384(6)	0.176(6)	0.132(6)	0.074(5)	3.750(45)	7.769(63)	5.654(100)	3.4
V18	18.955(4)	0.277(6)	0.131(6)	0.063(6)	0.061(6)	4.013(62)	8.205(114)	6.101(127)	4.5
V20	18.961(3)	0.305(4)	0.151(4)	0.109(4)	0.058(4)	3.978(39)	8.399(55)	6.497(91)	1.8
V21	18.910(3)	0.231(5)	0.104(5)	0.081(5)	0.041(5)	4.177(63)	8.721(87)	7.025(145)	3.7
V22	18.935(5)	0.375(7)	0.163(7)	0.128(8)	0.087(8)	3.909(61)	8.016(77)	6.000(106)	2.9
V23	18.797(6)	0.286(9)	0.146(8)	0.090(6)	0.053(7)	3.971(87)	8.208(143)	5.777(193)	3.6
V24	18.356(2)	0.133(3)	0.067(3)	0.038(3)	0.017(3)	4.058(68)	8.522(110)	6.766(203)	4.1
V25	18.844(3)	0.313(4)	0.139(4)	0.116(5)	0.077(4)	3.961(43)	8.157(56)	6.304(82)	1.6
V27	18.257(28)	0.219(40)	0.102(13)	0.052(30)	0.036(26)	4.385(590)	8.781(805)	6.254(1.000)	8.7
V29	18.975(4)	0.321(6)	0.171(6)	0.122(6)	0.080(6)	3.966(53)	8.082(76)	6.222(106)	2.3
V30	18.634(4)	0.239(5)	0.107(5)	0.087(5)	0.047(5)	3.761(64)	8.140(88)	5.908(132)	3.0
V31	18.901(6)	0.374(9)	0.124(9)	0.065(9)	0.053(9)	3.962(87)	7.694(158)	6.085(197)	9.2
V32	18.756(4)	0.248(5)	0.121(5)	0.088(5)	0.055(3)	3.814(60)	8.102(86)	5.883(121)	2.2
V33	19.032(4)	0.331(6)	0.151(6)	0.122(6)	0.088(5)	3.781(55)	8.142(77)	6.022(105)	4.2
V35	18.983(3)	0.261(4)	0.121(4)	0.085(4)	0.046(4)	4.096(47)	8.457(68)	6.601(112)	6.0
V38	18.837(3)	0.284(5)	0.142(5)	0.099(5)	0.056(5)	3.843(51)	8.179(74)	6.435(114)	3.0
V41	18.635(4)	0.290(6)	0.124(6)	0.093(6)	0.053(5)	3.752(58)	7.640(82)	5.719(132)	7.6
V43	18.944(4)	0.216(5)	0.100(5)	0.065(5)	0.033(5)	3.765(67)	8.320(103)	6.761(173)	6.3
V44	18.910(4)	0.291(5)	0.117(6)	0.077(6)	0.037(5)	3.965(63)	8.166(97)	6.195(178)	10.9
V45	18.903(3)	0.258(4)	0.119(4)	0.094(4)	0.054(4)	3.985(49)	8.378(69)	6.440(106)	4.4
V46	18.872(4)	0.120(5)	0.024(6)	0.015(6)	0.004(6)	5.010(295)	7.852(446)	5.724(1710)	20.5
V47	18.949(4)	0.273(5)	0.084(6)	0.044(6)	0.007(6)	3.953(77)	8.710(140)	7.822(828)	29.3
V48	18.967(3)	0.224(5)	0.136(5)	0.075(5)	0.040(5)	3.918(55)	8.471(89)	6.839(143)	2.4
V49	18.984(4)	0.287(6)	0.140(7)	0.093(6)	0.054(6)	3.877(59)	8.218(91)	6.396(139)	4.8
V50	18.919(4)	0.297(5)	0.154(5)	0.105(5)	0.071(5)	3.807(49)	8.217(72)	6.262(101)	4.3
V51	18.977(3)	0.156(4)	0.055(4)	0.036(4)	0.016(4)	4.283(88)	8.799(130)	7.095(279)	46.8
V52	18.938(3)	0.221(5)	0.089(5)	0.049(5)	0.029(5)	4.036(64)	8.550(108)	6.901(108)	1.8
V56	19.086(7)	0.391(10)	0.157(9)	0.147(8)	0.079(9)	3.650(79)	8.195(101)	5.826(153)	6.8
V58	18.851(3)	0.106(5)	0.029(5)	0.006(5)	0.008(5)	3.762(180)	8.572(800)	7.560(607)	32.1
V59	18.975(8)	0.392(13)	0.180(12)	0.110(11)	0.066(11)	3.934(85)	7.946(141)	5.616(215)	3.2
V60	18.913(4)	0.220(6)	0.096(6)	0.045(7)	0.028(6)	4.191(85)	8.439(141)	6.766(225)	1.8
V61	18.817(5)	0.369(7)	0.168(7)	0.086(8)	0.042(9)	4.163(57)	8.355(100)	5.796(172)	4.3
V63	18.801(7)	0.354(10)	0.147(10)	0.091(10)	0.053(10)	4.085(89)	8.325(139)	6.089(222)	4.0
V65	18.776(4)	0.221(6)	0.074(6)	0.056(6)	0.027(6)	3.940(95)	8.112(134)	6.501(235)	6.4
V67	18.508(4)	0.147(6)	0.082(6)	0.033(6)	0.009(5)	4.251(103)	9.072(205)	9.271(634)	42.4
V68	19.015(7)	0.296(10)	0.175(10)	0.128(10)	0.049(10)	4.072(91)	8.401(130)	6.709(245)	8.1
V69	19.422(14)	0.367(20)	0.370(19)	0.049(20)	0.048(20)	5.061(120)	7.556(422)	5.110(451)	22.6
V73	18.129(4)	0.173(5)	0.109(5)	0.052(5)	0.018(5)	3.915(79)	8.252(144)	5.891(317)	7.8
V76	19.118(8)	0.446(12)	0.221(12)	0.118(12)	0.027(12)	4.297(77)	9.032(138)	6.932(483)	11.1
RRC									
V53	18.837(3)	0.103(4)	0.014(4)	0.020(4)	0.004(4)	3.013(300)	5.230(226)	3.169(884)	
V57	18.956(4)	0.305(5)	0.035(5)	0.033(5)	0.006(5)	4.894(162)	4.041(166)	1.904(813)	
V62	18.873(4)	0.211(5)	0.028(6)	0.029(5)	0.004(5)	4.646(174)	2.827(187)	1.485(1152)	
V64	18.877(4)	0.179(5)	0.046(5)	0.021(5)	0.011(5)	3.438(124)	1.770(253)	5.366(474)	
V71	18.703(4)	0.205(6)	0.045(5)	0.024(5)	0.013(5)	4.443(145)	1.300(266)	5.283(449)	

The numbers in parenthesis indicate the uncertainty on the last decimals.

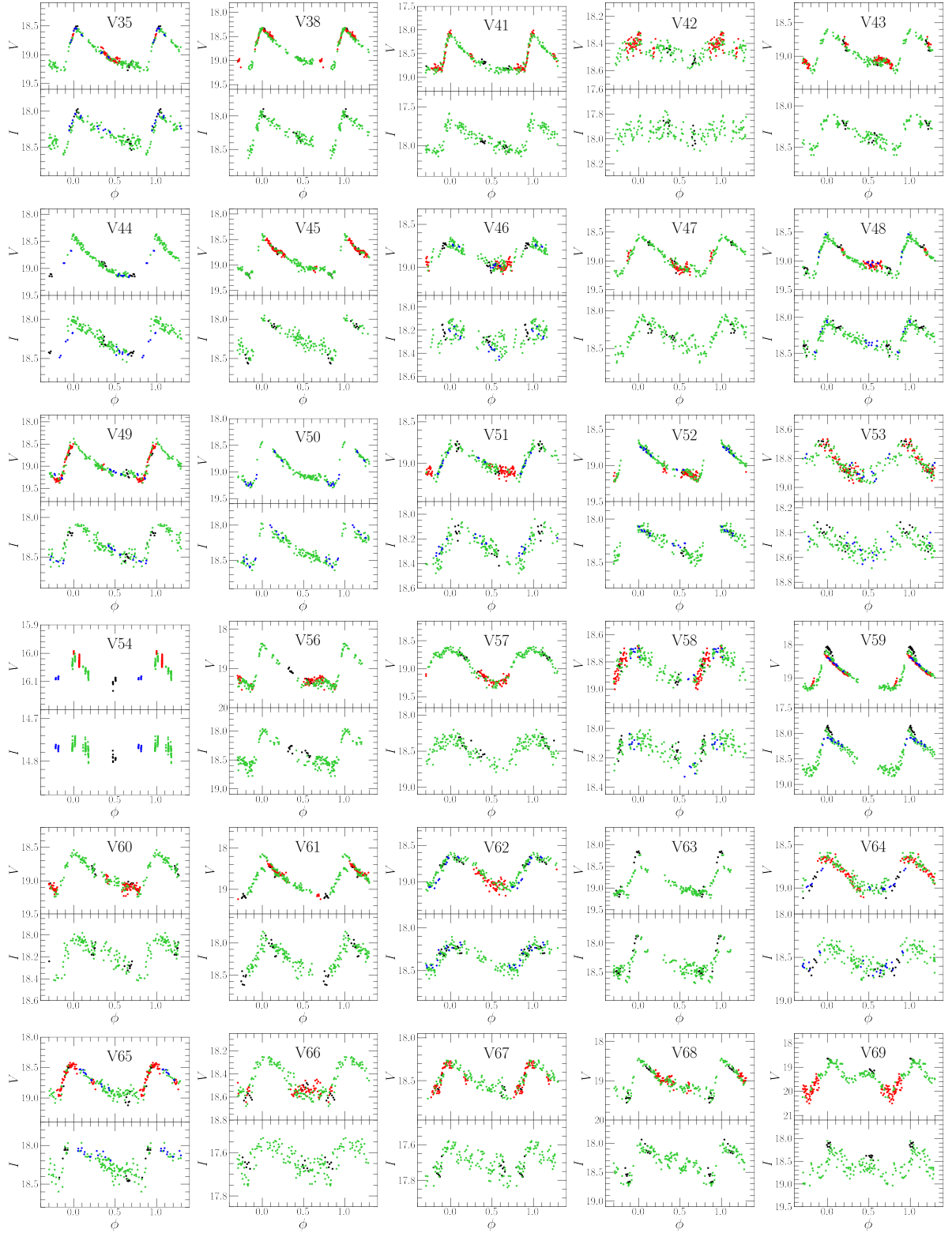
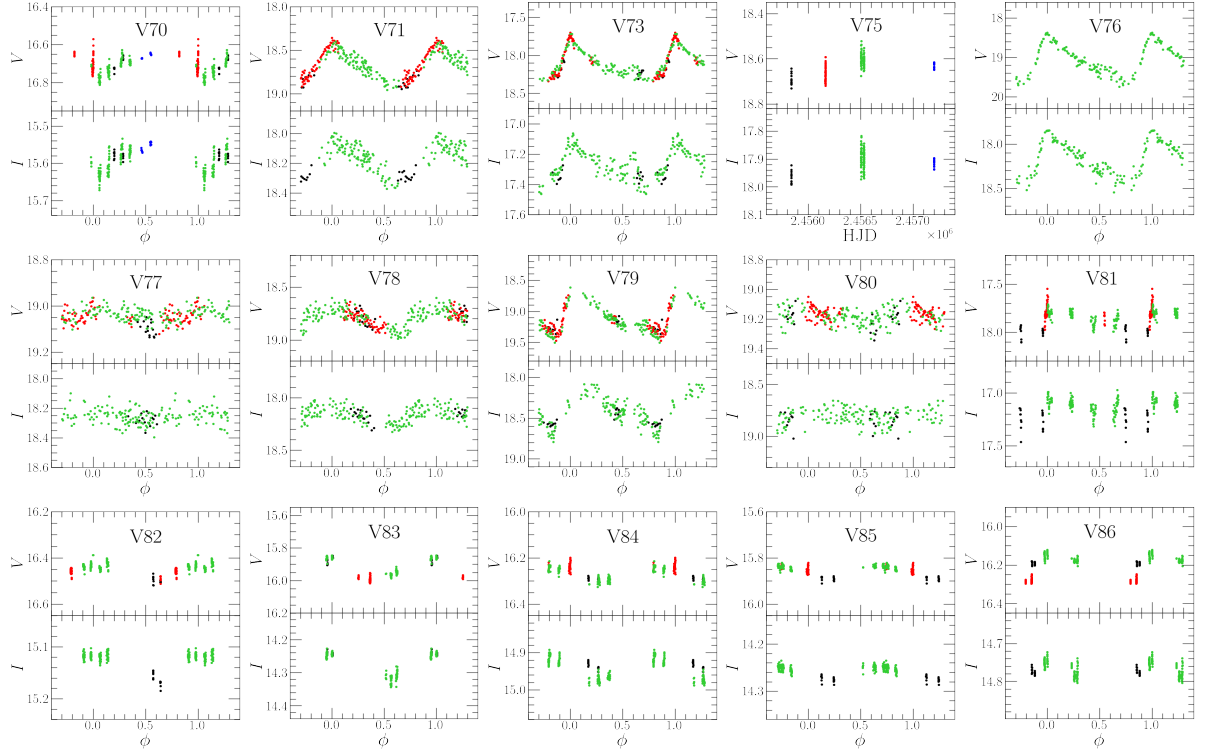


Figure 3. continued

by the calibration of [Nemec et al. \(2013\)](#) scale, $[\text{Fe}/\text{H}]_{\text{Nem}}$, also in the spectroscopic metallicity scale.

The estimated weighted mean values are also indicated in the bottom of the table. For $[\text{Fe}/\text{H}]_{\text{UVES}}$ we found -1.41 ± 0.13 and -1.75 ± 0.27 from RRab and RRc stars respectively.

The mean cluster distance is estimated from the individual values of the absolute magnitude M_V and the corresponding distances for a reddening $E(B - V) = 0.08$. An average distance of 41.1 ± 1.5 kpc is found from RRab stars and a very similar value for RRc stars.

**Figure 3.** continued

5.1.1 Cluster distance from P-L(*I*) relationship

An independent instrument to calculate the distance of globular cluster with RR Lyrae stars is the P-L relationship in the *I* band of [Catelan \(2004\)](#); $M_I = 0.471 - 1.132 \log P + 0.205 \log Z$, where P is the fundamental period, $\log Z =$

$[M/H] - 1.765$, $[M/H] = [Fe/H] - \log(0.638f + 0.205)$ and $\log f = [\alpha/Fe]$ ([Salaris et al. 1993](#)).

For the calculation of the distance via P-L(*I*) relation we have employed the intensity weighted mean magnitude $\langle I \rangle$ (see Table 3), $E(B - V) = 0.08$ and $E(V - I) = 1.259E(B - V)$. We applied this P-L equation to 44 RRab stars given

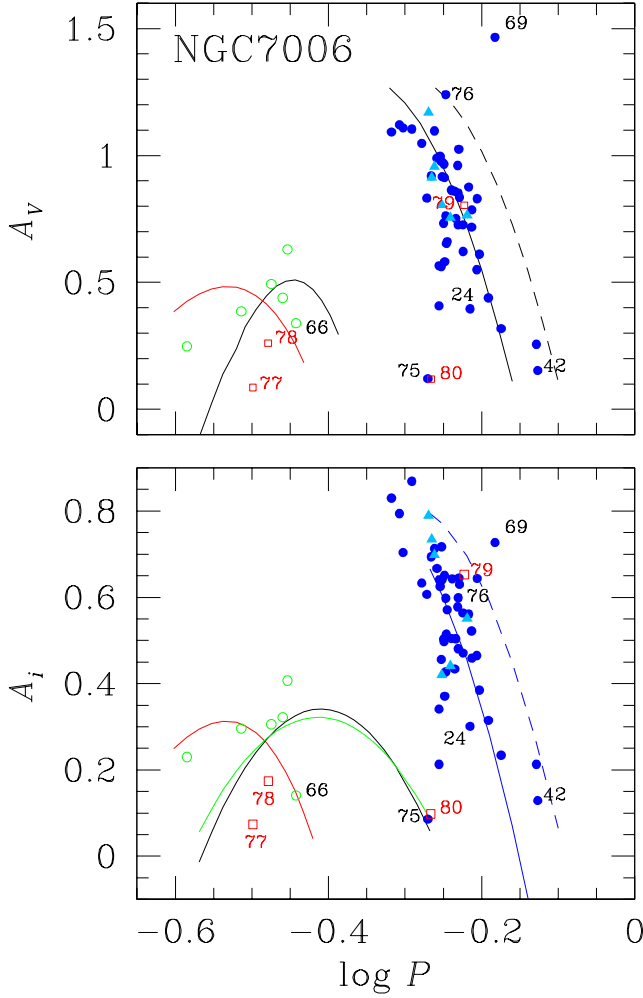


Figure 4. Period-Amplitude plane in V (top) and I (bottom) filters for NGC 7006. Blue and green symbols represent RRab and RRC stars respectively. The stars that present Blazhko-like amplitude modulations are marked with light blue triangles. The empty red squares indicate the new variables announced in the present work. In the top panel, the continuous and segmented black loci represent the distribution of unevolved and evolved stars, respectively, in M3 according to (Cacciari et al. 2005). Kunder et al. (2013a) found the black parabola for the RRC stars from 14 OoII clusters. Arellano Ferro et al. (2015) calculated the red parabolas from a sample of RRC stars in five OoI clusters, excluding variables with Blazhko effect. In the bottom panel, the continuous and segmented blue lines were constructed by Kunder et al. (2013b). The green parabola was calculated by Deras et al. (2019) from RRC stars in M13 and the black one by Yepez et al. (2020), using 28 RRC stars from seven OoII clusters.

their fundamental period P_0 . Four RRC stars were also included after fundamentalizing their period assuming the ratio $P1/P0 = 0.749$. The resulting mean distance for these 48 RR Lyrae is 40.2 ± 1.2 kpc, in quite a good agreement with the results from the Fourier decomposition (Table 5).

6 THE COLOUR MAGNITUDE DIAGRAM OF NGC 7006

Fig. 5 displays the CMD of NGC 7006 built based on the VI photometry of the work. The top left panel display the distribution of all stars measured in the field of NGC 7006, and distinguishes the field and member stars resulting from the analysis of § 3. The top right panel displays the variable stars distribution on the unreddened plane $(V - I)_0 - V_0$. All theoretical loci have been placed at a distance of 44.0 kpc, since we found this to produce the best representation of the stellar distribution. We should note the small difference with the distance obtained from the Fourier RR Lyrae light curve decomposition (Table 5) and from the P-L(I) relation, which is 40.2 ± 1.2 kpc. The difference is the consequence of the RR Lyrae being intrinsically brighter than ZAHB due to evolutionary reasons. The bottom panel of Fig. 5 is an expansion of the HB region that helps studying in detail the distribution of the RR Lyrae stars. Several aspects should be highlighted from this plot: first, we note that all variables (coloured symbols as coded in the figure caption) matching a cluster member star (black points) carry a black dot in the center, the absence of which means that the star was found to be likely a field star by our approach of § 3, (see for example the cases of V27, V67 and V73 among others). Second, a few R Rab and R R c stars are at an odd position, either too luminous for a cluster member at the HB, or in the "wrong" side of the first overtone red edge (FORE). This could be due to the fact that the star is not a cluster member (e.g. V27 and V73) or that in our images the star is blended with a brighter star (e.g. V30, V69). In Appendix A we include comments on peculiar stars. It is worth mentioning that all the non-peculiar R Rab and R R c concentrate near the ZAHB and the two modes are well separated by the FORE, i.e., no R Rab stars are found in the multi-mode region just to the blue of the FORE. This circumstance, that is a common feature in OoII clusters, has been identified only in some OoI clusters (e.g. Yepez et al. 2022), and this seems to be the case of NGC 7006. The solid tilted red and blue lines are our empirical estimates of the fundamental mode and the first overtone instability strip edges respectively. For comparison we have included the theoretical instability strip bounds calculated by Bono et al. (1994) (their Figure 4) converted from the $\log T_{\text{eff}} - \log L$ plane to the $(V - I)_0 - V_0$ observational plane. This was achieved by adopting the cluster distance 41.2 kpc and the T_{eff} vs $(V - I)_0$ described by Arellano Ferro et al. (2010).

7 ON THE PROGENITORS OF RR LYRAE AND BL HER STARS

We would like to understand which stars evolved to become the RR Lyrae stars in NGC 7006. Similarly we would like to explain the progenitor of stars like the BL Her type V81 in NGC 7006. For both purposes we have employed the Eggleton code (Pols et al. 1997, 1998; Schröder et al. 1997) and a modified mass loss Reimers law (Schröder & Cuntz 2005) to produce ZAHBs models for different He core and envelope masses.

Theoretical calculations of post-HB evolution have been carried out by several authors using different codes (e.g. Osborn et al. 2019; Bono et al. 2020; Yepez et al. 2022). All

Table 5. Physical parameters for the RR Lyrae stars calculated using Fourier decomposition parameters and well-defined empirical calibrations.

Variable	[Fe/H] _{ZW}	[Fe/H] _{UVES}	[Fe/H] _{Nem}	M_V	$\log T_{\text{eff}}$	$\log(L/L_{\odot})$	D (kpc)	M/M_{\odot}	R/R_{\odot}
RRab									
V1	-1.49(5)	-1.40(6)	-1.28	0.64(1)	3.831	1.646(3)	40.13(13)	0.61(1)	4.86(2)
V2 ^a	–	–	–	0.55(1)	3.810	1.681(3)	42.09(16)	0.67(1)	5.59(2)
V3	-1.39(7)	-1.29(7)	-1.12	0.59(1)	3.793	1.662(3)	41.72(14)	0.83(1)	5.90(2)
V5	-1.55(10)	-1.48(11)	-1.46	0.64(1)	3.820	1.643(4)	38.87(19)	0.61(1)	5.09(2)
V6 ^a	–	–	–	0.62(1)	3.812	1.653(4)	42.47(21)	0.77(1)	5.35(3)
V10 ^a	–	–	–	0.52(1)	3.819	1.691(4)	43.10(20)	0.70(1)	5.42(3)
V11 ^a	–	–	–	0.60(1)	3.797	1.660(3)	41.91(14)	0.76(1)	5.79(2)
V12	-1.94(10)	-2.01(14)	-2.42	0.61(1)	3.803	1.657(3)	40.65(16)	0.70(1)	5.61(2)
V13	-1.65(8)	-1.60(9)	-1.67	0.61(1)	3.809	1.655(4)	41.56(19)	0.69(1)	5.43(2)
V14	-1.53(6)	-1.44(7)	-1.39	0.61(1)	3.798	1.656(4)	41.66(17)	0.76(1)	5.72(2)
V15	-1.66(7)	-1.61(8)	-1.66	0.57(1)	3.795	1.671(3)	40.98(12)	0.77(1)	5.91(2)
V16	-1.42(9)	-1.32(10)	-1.18	0.61(1)	3.795	1.655(6)	39.77(26)	0.84(1)	5.80(4)
V17	-1.71(6)	-1.68(8)	-1.81	0.62(1)	3.821	1.652(3)	41.03(16)	0.66(1)	5.12(2)
V18	-1.65(11)	-1.60(13)	-1.63	0.55(1)	3.796	1.679(3)	42.76(17)	0.75(1)	5.95(2)
V20	-1.37(5)	-1.26(5)	-1.06	0.59(1)	3.811	1.662(2)	42.06(11)	0.64(1)	5.42(1)
V21	-1.20(8)	-1.08(7)	-0.71	0.61(1)	3.787	1.657(3)	40.82(13)	0.76(1)	6.02(2)
V22	-1.54(7)	-1.46(8)	-1.42	0.60(1)	3.815	1.659(4)	41.38(20)	0.69(1)	5.31(3)
V23	-1.66(13)	-1.61(16)	-1.65	0.56(1)	3.805	1.676(5)	39.61(21)	0.66(1)	5.67(3)
V25	-1.47(5)	-1.37(6)	-1.27	0.64(1)	3.849	1.644(2)	39.01(11)	0.42(1)	4.46(1)
V31 ^a	–	–	–	0.50(1)	3.749	1.701(5)	42.75(25)	1.54(2)	7.57(4)
V32	-1.59(8)	-1.52(9)	-1.53	0.66(1)	3.822	1.634(3)	37.05(12)	0.54(1)	4.99(2)
V33	-1.53(7)	-1.45(8)	-1.41	0.61(1)	3.785	1.658(3)	43.26(17)	0.91(1)	6.10(2)
V35 ^a	–	–	–	0.60(1)	3.788	1.660(2)	42.39(11)	0.79(1)	6.02(2)
V38	-1.77(7)	-1.73(9)	-1.83	0.55(1)	3.818	1.681(3)	40.56(13)	0.55(1)	5.36(2)
V43 ^a	–	–	–	0.64(1)	3.803	1.646(3)	40.95(13)	0.64(1)	5.54(2)
V45	-1.41(7)	-1.31(7)	-1.14	0.63(1)	3.788	1.649(2)	40.33(11)	0.80(1)	5.96(2)
V46 ^a	–	–	–	0.61(1)	3.806	1.656(3)	40.06(14)	0.54(1)	5.51(2)
V47 ^a	–	–	–	0.59(1)	3.805	1.663(3)	41.87(15)	0.71(1)	5.60(2)
V48	-1.43(8)	-1.33(9)	-1.14	0.61(1)	3.790	1.655(3)	41.82(14)	0.74(1)	5.93(2)
V49	-1.56(9)	-1.48(10)	-1.44	0.60(1)	3.799	1.662(3)	42.48(17)	0.73(1)	5.75(2)
V51 ^a	–	–	–	0.62(1)	3.774	1.653(2)	41.91(11)	0.82(1)	6.36(2)
V52	-1.40(19)	-1.29(10)	-1.04	0.58(1)	3.783	1.668(3)	41.86(14)	0.82(1)	6.23(2)
V56	-1.45(10)	-1.35(10)	-1.23	0.57(1)	3.775	1.673(5)	45.07(28)	1.09(2)	6.49(4)
V58	-1.84(75)	-1.85(98)	-1.63	0.53(1)	3.782	1.687(3)	41.12(13)	0.67(1)	6.38(2)
V59	-1.43(13)	-1.33(14)	-1.15	0.64(2)	3.831	1.643(7)	41.39(33)	0.63(1)	4.85(4)
V60	-1.52(13)	-1.43(14)	-1.28	0.57(1)	3.774	1.670(4)	41.52(17)	0.90(1)	6.50(3)
V61	-1.46(10)	-1.36(10)	-1.22	0.49(1)	3.825	1.706(4)	41.37(20)	0.60(1)	5.36(3)
V63	-1.33(13)	-1.21(13)	-1.00	0.57(1)	3.833	1.674(6)	39.57(26)	0.55(1)	4.97(3)
V68 ^a	–	–	–	0.65(1)	3.783	1.640(6)	42.01(27)	0.89(1)	6.03(4)
Weighted Mean	-1.53(1)	-1.43(1)	-1.41	0.597(1)	3.802	1.660(1)	41.17(22)	0.67(1)	5.61(1)
σ	± 0.15	± 0.20	± 0.33	± 0.040	± 0.020	± 0.016	± 1.39	± 0.18	± 0.56
RRc									
V53	-1.59(34)	-1.52(38)	–	0.73(2)	3.882	1.609(9)	37.33(38)	0.50(1)	3.68(4)
V57	-1.52(34)	-1.44(37)	-1.43(27)	0.55(2)	3.853	1.681(9)	42.87(47)	0.55(2)	4.57(5)
V62	-1.99(36)	-2.08(51)	-2.01(24)	0.57(2)	3.827	1.671(9)	40.78(45)	0.74(2)	5.09(6)
V64	-1.99(43)	-2.09(61)	-1.83(25)	0.64(2)	3.879	1.646(9)	39.70(42)	0.45(1)	3.90(4)
V71	-2.09(46)	-2.24(67)	-2.03(25)	0.55(2)	3.833	1.679(9)	38.05(41)	0.78(2)	5.00(5)
Weighted Mean	-1.79(16)	-1.72(21)	-1.84(10)	0.61(1)	3.853	1.656(4)	39.49(19)	0.55(1)	4.27(2)
σ	± 0.27	± 0.27	± 0.28	± 0.07	± 0.022	± 0.027	± 2.22	± 0.13	± 0.57

a: These variables are not included in the calculation of [Fe/H] since their D_m parameter is larger than 5.0

The numbers in parentheses indicate the uncertainty on the last decimal place.

these studies agree that globular cluster cepheids or BL Her stars, have their progenitors from the blue tail of the ZAHB as their He-core get exhausted, and may have total masses in the range 0.52-0.58 M_{\odot} for a canonical helium abundance of $Y=0.25$. [Osborn et al. \(2019\)](#), studying the secular period

changes, found that in a sample of 18 BL Her stars, all have positive period changes, i.e. they are all evolving redwards, and that depending upon their period they may be in the first redward crossing of the instability strip or the second redward crossing (after the He shell flashes in the AGB that

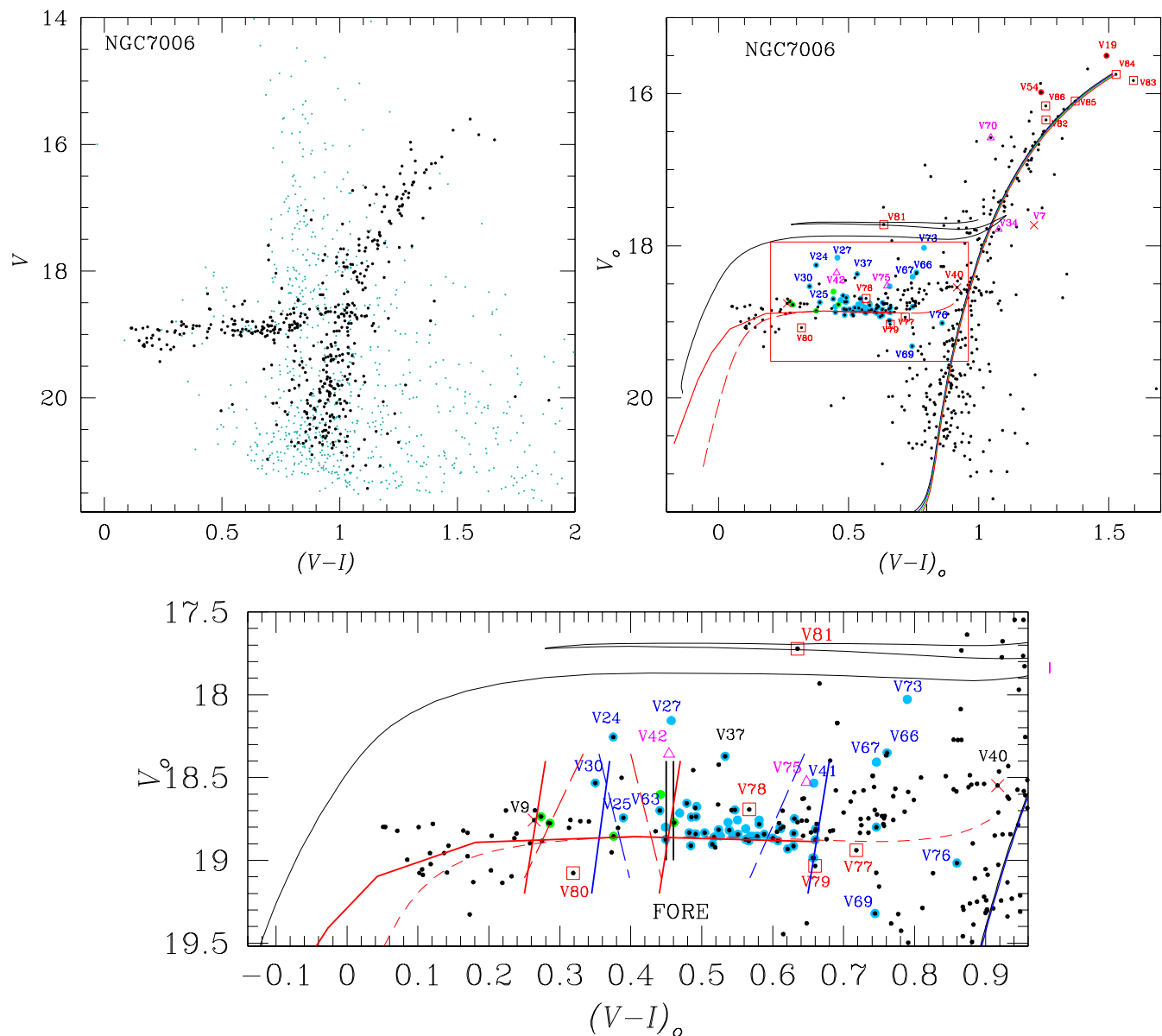


Figure 5. CMD of NGC 7006 and the variable stars distribution. The top left panel shows the all stars measured by our photometry. Light green and black dots represent the field stars and the likely cluster members respectively (§ 3). The top right panels is the unreddened CMD with the variable stars identified. The dashed ZAHB and isochrones for 12.0 to 13.5 Gyrs and $[\text{Fe}/\text{H}]=-1.58$, $Y = 0.25$ and $[\alpha/\text{Fe}]=+0.4$ are from the models of [VandenBerg et al. \(2014\)](#). The continuum ZAHB is from the models built from the Eggleton code ([Pols et al. 1997, 1998; Schröder et al. 1997](#)), and calculated by [Yepez et al. \(2022\)](#). The black continuous line is an evolutionary track of a star starting in the blue tail of the HB, with a core and total masses of 0.49 and 0.55 M_{\odot} respectively. This track represents well the BL Her star V81. All theoretical loci were placed at a distance of 44 kpc that was found to provide the best fits. The red square is magnified in the bottom panel where the variable stars are coded as: RRab blue, RRc green, SR red, magenta triangles are for stars of confirmed variability in this work, crosses for variables not confirmed by our photometry. Red squares mark the newly found variables. Tilted continuous blue and red lines represent our empirical estimates of the fundamental mode and the first overtone instability strip edges respectively. For comparison the theoretical lines from [Bono et al. \(1994\)](#) (their Figure 4) are shown with broken lines (see the text for details). The vertical black lines are the empirical First Overtone Red Edge (FORE) from [Arellano Ferro et al. \(2015, 2016\)](#).

produce the blue loops). No stars with blueward evolution (negative period changes) were found. Comparison with theory allow these authors to conclude that BL Her stars have helium abundances close to the canonical $Y=0.25$ and that values as large as 0.33 can be excluded. In the characterization of the evolution of BL Her and W Vir stars made by [Bono et al. \(2020\)](#), we learn that BL Her are post-early asymptotic

giant branch (PEAGB) stars with masses $0.495 < M_{\odot} < 0.55$ evolving along their first crossing towards the AGB, while W Vir stars are a mix of PEAGB and post-AGB stars (hydrogen shell burning). [Yepez et al. \(2022\)](#) have pointed out that models with $M > 0.54 M_{\odot}$ can represent BL Her stars only if the mass of the envelope is small.

The continuous ZAHB in Fig. 5 was obtained for models

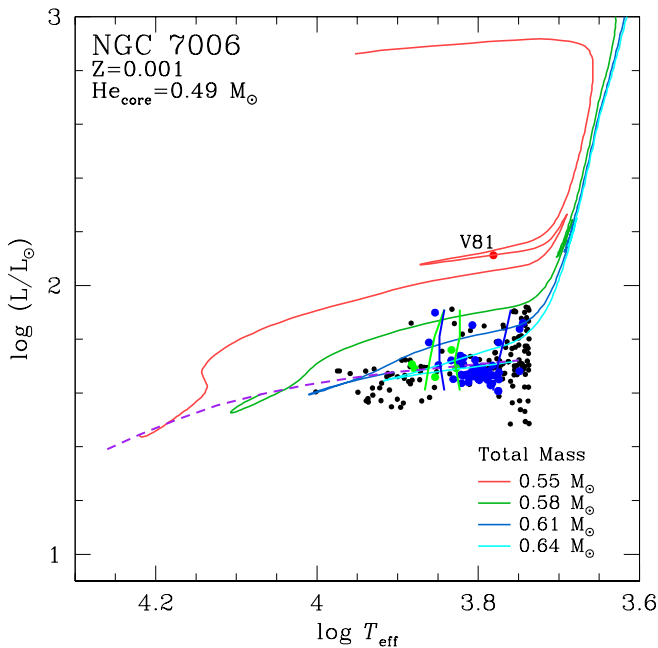


Figure 6. HR diagram of the HB of NGC 7006. The evolutionary tracks were calculated for a core mass of $0.49 M_{\odot}$ and the total masses in the legend. Only configurations with thin a envelope ($0.06 M_{\odot}$) would have sufficient luminosity to represent the BL Her star V81. Massive envelopes also do not produce blue loops. Blue and green nearly vertical lines are the theoretical instability strip borders for the fundamental and first overtone respectively, taken from [Bono et al. \(1994\)](#).

with a core mass of $0.49 M_{\odot}$ and total mass in the range 0.55 – $0.64 M_{\odot}$. Notice that larger core masses would naturally produce more luminous ZAHB's. The dashed ZAHB is from the models of [VandenBerg et al. \(2014\)](#) for an initial core mass of $0.49 M_{\odot}$. Our models indicate that a main sequence star with a mass between 0.82 and $0.85 M_{\odot}$ would reach the RGB in 12 to 13.5 Gyrs. When progenitors within this mass range reach the ZAHB they have lost between 25–35% of their mass due to He-flash events at the RGB. The continuous black line in Fig. 5, is an evolutionary track starting at the blue end of the HB and rising to the position of the BL Her star V81. This model has a core mass of $0.49 M_{\odot}$ and a total mass of $0.55 M_{\odot}$, i.e. a very thin envelope of $0.06 M_{\odot}$.

Fig. 6 shows the HR diagram of NGC 7006 and our models for a core mass of $0.49 M_{\odot}$ and envelope masses in the range 0.06 – $0.15 M_{\odot}$. Models with massive envelopes will remain at luminosities much lower than that of the V81 and will not produce blue loops. We have also found for the cases of Pop II Cepheids in M14 ([Yepez et al. 2022](#)) and M10 ([Arellano Ferro et al. 2020](#)), that these thin envelopes are necessary to explain BL Her and W Virginis with low mass predecessors from the blue tail of the HB.

8 SUMMARY OF RESULTS

Accurate *VI* magnitudes were extracted for 1373 star in the field of NGC 7006. Using the *Gaia*-DR3 accurate sky positions and proper motions we have separated 470 stars that are likely cluster members. This enabled us to build a clean CMD

and discuss its structure and further improve the membership status of the population of variable stars. In this process we have explored the light curves of all our photometric sources and discovered 10 new variables; 2 RRab, 2 RRc, 1 CWB and 5 SR. The coordinates and classifications of a few variables were corrected, e.g. the cases of the two CW stars V70 and V81. A few variables in the FoV of the clusters on close scrutiny were found to be field stars. The cluster is confirmed as of the Oo I type.

The $(V - I)$ colour curves of RRab stars is known to be constant. We have taken advantage of that to estimate the reddening of the cluster as 0.08 ± 0.05 . The light curves of the confirmed RR Lyrae members were Fourier decomposed and their physical parameter were calculated. We provide the Fourier parameters as well as the individual physical parameters, effective temperatures, masses and radii besides the metallicity and distance. The RRab stars lead to the mean cluster metallicity and distance of $[\text{Fe}/\text{H}]_{\text{ZW}} = -1.53 \pm 0.15$ and 41.2 ± 1.4 kpc.

The CMD diagram displays the distribution of variable members in good concordance with theoretical loci, i.e. ZAHB and isochrones placed at the resulting distance. We notice the presence of RRab stars in the multi mode-region of the HB, which is a common feature in some Oo I clusters.

The employment of evolutionary models that use the Eggleton code, allowed us to estimate the mass of the HB stars predecessors at the main sequence to be in the range 0.82 and $0.85 M_{\odot}$ and to infer that by the time these stars reach the HB, 12–13.5 Gyrs later they may have lost 25–35% of the mass. Likewise, the models enabled us to demonstrate that CW stars (BL Her or W Virginis stars) can be explained by stars evolved from the blue tail of the HB provided that the envelope is thin ($\sim 0.06 M_{\odot}$), or in other words with a large core to total mass ratio.

ACKNOWLEDGEMENTS

AAF acknowledges the financial support of the program m PAPIIT, UNAM, through grant IG100620. FCRG is grateful to CONACyT (Mexico) for a M. Sc. scholarship. We thank the staff of the IAO, Hanle and CREST, Hosakote, for making these observations possible. The facilities at IAO and CREST are operated by the Indian Institute of Astrophysics, Bangalore. We have made extensive use of the SIMBAD and ADS services, for which we are thankful.

DATA AVAILABILITY

The data underlying this article shall be available in an electronic form in the Centre de Données astronomiques de Strasbourg data base (CDS), and can also be shared on request to the corresponding author.

REFERENCES

- Allen C., Moreno E., Pichardo B., 2006, *ApJ*, **652**, 1150
- Arellano Ferro A., 2022, *RMA&A*, **58**, 257
- Arellano Ferro A., Giridhar S., Bramich D. M., 2010, *MNRAS*, **402**, 226

Arellano Ferro A., Mancera Piña P. E., Bramich D. M., Giridhar S., Ahumada J. A., Kains N., Kuppuswamy K., 2015, *MNRAS*, 452, 727

Arellano Ferro A., Luna A., Bramich D. M., Giridhar S., Ahumada J. A., Muneer S., 2016, *Ap&SS*, 361, 175

Arellano Ferro A., Yepez M. A., Muneer S., Bustos Fierro I. H., Schröder K. P., Giridhar S., Calderón J. H., 2020, *MNRAS*, 499, 4026

Bono G., Caputo F., Stellingwerf R. F., 1994, *ApJ*, 423, 294

Bono G., et al., 2020, *A&A*, 644, A96

Bramich D. M., 2008, *MNRAS*, 386, L77

Bramich D. M., Figuera Jaimes R., Giridhar S., Arellano Ferro A., 2011, *MNRAS*, 413, 1275

Bramich D. M., et al., 2013, *MNRAS*, 428, 2275

Burke Edward W. J., Rolland W. W., Boy W. R., 1970, *J. R. Astron. Soc. Canada*, 64, 353

Bustos Fierro I. H., Calderón J. H., 2019, *MNRAS*, 488, 3024

Cacciari C., Corwin T. M., Carney B. W., 2005, *AJ*, 129, 267

Carretta E., Bragaglia A., Gratton R., D'Orazi V., Lucatello S., 2009, *A&A*, 508, 695

Catelan M., 2004, *ApJ*, 600, 409

Clement C. M., et al., 2001, *AJ*, 122, 2587

Cox A. N., Hodson S. W., Clancy S. P., 1983, *ApJ*, 266, 94

Deras D., Arellano Ferro A., Lázaro C., Bustos Fierro I. H., Calderón J. H., Muneer S., Giridhar S., 2019, *MNRAS*, 486, 2791

Dworetzky M. M., 1983, *MNRAS*, 203, 917

Gaia Collaboration et al., 2021, *A&A*, 649, A1

Gerashchenko A., 2006, *Peremennye Zvezdy*, 26, 1

Gerashchenko A. N., Ananjevskaja Y. K., 2018, *Astrophysics*, 61, 182

Guldenschuh K. A., et al., 2005, *PASP*, 117, 721

Jurcsik J., Kovacs G., 1996, *A&A*, 312, 111

Kunder A., et al., 2013b, *AJ*

Kunder A., Stetson P. B., Catelan M., Walker A. R., Amigo P., 2013a, *AJ*

Nemec J. M., Cohen J. G., Ripepi V., Derekas A., Moskalik P., Sesar B., Chadid M., Bruntt H., 2013, *ApJ*, 773, 181

Netzel H., Smolec R., 2022, *MNRAS*, 515, 3439

Osborn W., Kopacki G., Smith H. A., Layden A., Pritzl B., Kuehn C., Anderson M., 2019, *Acta Astron.*, 69, 101

Pinto G., Rosino L., 1973, *Mem. Soc. Astron. Italiana*, 44, 255

Pols O. R., Tout C. A., Schroder K.-P., Eggleton P. P., Manners J., 1997, *MNRAS*, 289, 869

Pols O. R., Schröder K.-P., Hurley J. R., Tout C. A., Eggleton P. P., 1998, *MNRAS*, 298, 525

Rosino L., Ciatti F., 1967, *Asiago-Padova Cont.*, 5, No. 199

Salaris M., Chieffi A., Straniero O., 1993, *ApJ*, 414, 580

Schlafly E. F., Finkbeiner D. P., 2011, *ApJ*, 737, 103

Schlegel D. J., Finkbeiner D. P., Davis M., 1998, *ApJ*, 500, 525

Schröder K. P., Cuntz M., 2005, *ApJ*, 630, L73

Schröder K.-P., Pols O. R., Eggleton P. P., 1997, *MNRAS*, 285, 696

Stetson P. B., 2000, *PASP*, 112, 925

Sturch C., 1966, *ApJ*, 143, 774

VandenBerg D. A., Bergbusch P. A., Ferguson J. W., Edvardsson B., 2014, *ApJ*, 794, 72

Wehlau A., Nemec J. M., Hanlan P., Rich R. M., 1992, *AJ*, 103, 1583

Wehlau A., Slawson R. W., Nemec J. M., 1999, *AJ*, 117, 286

Yepez M. A., Arellano Ferro A., Deras D., 2020, *MNRAS*, 494, 3212

Yepez M. A., Arellano Ferro A., Deras D., Bustos Fierro I., Muneer S., Schröder K. P., 2022, *MNRAS*, 511, 1285

Zinn R., West M. J., 1984, *ApJS*, 55, 45

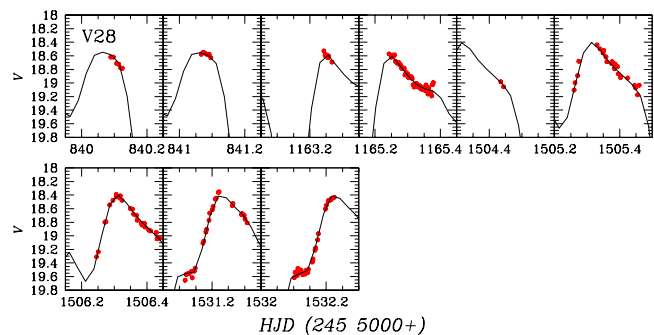


Figure A1. V28 V data phased with a double mode model with periods 0.33213 and 0.49914 d.

APPENDIX A: COMMENTS ON INDIVIDUAL STARS

Here we address a few stars whose light curve, classification, identification, membership status or position in the CMD display some peculiarity.

V7 and V40. These two star, identified with a cross in Fig. 5, do not show variations in our data. V7 is in fact labeled as a non variable in the CVSGC.

V24. This RRab star appears as a likely cluster member, in spite of which it is too luminous in the DCM. Furthermore the P-L(*I*) relation gives a distance of 31.8 kpc. Therefore the star is likely a foreground star.

V26, V37, V39, V55. These stars we not measured by our photometry because they are to faint and/or blended in a crowded region. V55 is out of out FoV.

V27, V41 and V73. These stars are found to be field stars. Their position in the CMD is in fact peculiar, being too luminous to pertain to the HB, hence we consider this star as non cluster members.

V28. This star has been classified as RRab in the CVSGC with a period of 0.4970 d. However our data are not phased at all by this period and rather suggest a period of 0.3321 d. We have processed our data through a double mode model analysis and find two simultaneous active periods of 0.33213 and 0.49914 d which, if interpreted as the first overtone and fundamental periods have a ratio $P1/P0 = 0.665$. This value is substantially smaller than the canonical 0.746 ratio (Cox et al. 1983) for RRd stars. It seems clear that the star is double mode pulsator, but our data are rather insufficient for a more accurate evaluation of the involved modes, periods and their ratio. In Fig. A1 the V data of V28 are fitted by a double mode wave of the above periods. The representations is quite satisfactory but we recognize that our data are scarce for further analysis. We can only comment at present that, although the period ratio 0.665 is larger than in the recently discussed double mode stars with excited harmonics of non-radial modes, 0.61 (Netzel & Smolec 2022), the star is worth an analysis when more observations of good quality are available.

V30. The star is listed in the CVSGC as non variable. We found the coordinates listed there were off by a few arc seconds and corrected the coordinates. At the correct position we find a clear RRab. The star is nevertheless too luminous in the DCM and we doubt its membership status. Hence, it was not used for the Fourier analysis.

V34. Related with the controversy on the identification and variability of this star, the reader can refer to the note in the CVSGC (Clement et al. 2001) (2015 edition). Here we were guided by the coordinates given in this catalogue and the identification chart of Wehlau et al. (1992), that in fact coincide. This star is obviously brighter than cluster RR Lyrae stars by more than one magnitude. In our data the star presents a sinusoidal mild variation with period of 0.9088 days. In the CMD it is found in the RGB. The membership analysis identifies it as a cluster member. In our opinion the star may be a binary star probably of the EW type.

V36, V66, V72. These three stars form a group and are badly blended in our images. We could only isolate a reasonable light curve for V66. In the CVSGC the quoted period for V66 is 0.6172 d, however we found it to be better phased with 0.3557 d, suggesting we are dealing with a RRc star. Nevertheless, the mutual light contamination of this group makes them all unsuitable for proper analysis. Thus we refrain from further comments on the nature of V66. This circumstance also explains the odd position of V66 in the DCM.

V42. This star is very close to the cluster center in a crowded region. It is near to a much brighter star. The present data are apparently the first ever published. Our light curve is scattered, nonetheless the period suggests the star being an R Rab. The membership analysis finds the star to be a field star.

V60, V67. These stars were classified as RRc stars in the CVSGC. We found periods and light curve shapes typical of RRab stars hence we reclassified them. V67 appears to be red and too luminous relative to the HB. It is also found not to be a cluster member and its distance via the P-L(*I*) relation is much too short.

V68, V69. These stars had no Bailey type in the CVSGC. We found periods and light curve shapes typical of RRab stars hence we reclassified them. V69, in spite of having been selected as a likely cluster member by the membership analysis, in the DCM appears much below the HB. Also, the P-L(*I*) relation renders a distance of 50.3 kpc, hence the star seems to be behind the cluster.

V70. This star carries a note in the CVSGC indicating that the star is probably not a RR Lyrae star (Pinto & Rosino 1973). Its position on the CMD is much brighter than the HB and towards the RGB. We find the star to be a cluster member. Our data are properly phased with a period of 11.7 d. Given its position on the CMD and its period the star could well be a W Virginis or CW star.

V75. No short term variations were detected for this star by Wehlau et al. (1999). Our light curve is noisy but in the *V* vs HJD plane it displays clear variations in both *V* and *I* bands, with an amplitude of about 0.1 mag. A period search finds 13.5071 d. and the phased light curves can be seen in Fig. A2. We agree with Rosino & Ciatti (1967) that that it is not an RR Lyrae. Its position slightly above the HB and its period suggest that it is a CWA or W Virginis star somewhat behind the cluster.

V76. This faint RRab may be subject to light and colour contamination from its brighter neighbour V31. The star appears too red and fainter than most RRab's on the HB which may indicate that the star does not belong to the cluster in spite to have been identified as a likely member by our membership analysis.

V1, V11, V12, V13, V14, V16, V27, V41, V42, V44, V45,

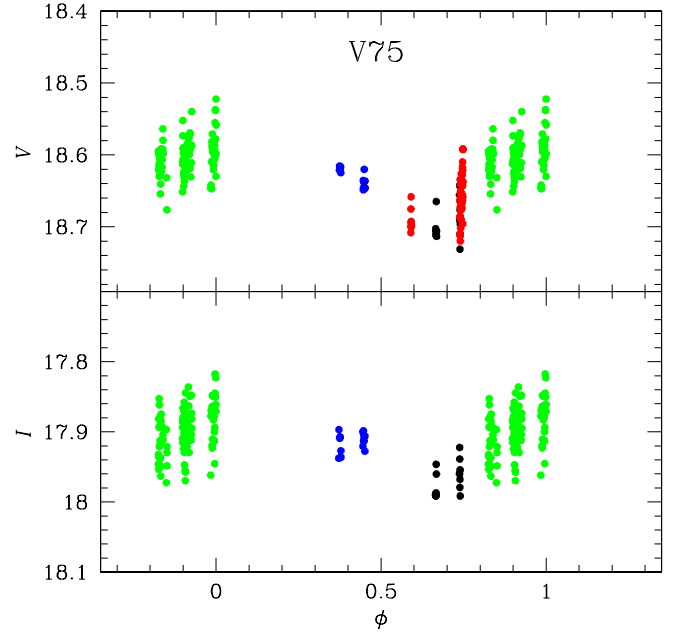


Figure A2. V75 phased with $P=13.5071$ d, which along with its position in the DCM suggests the star to be a W Virginis (CWA) slightly behind the cluster.

V46, V47, V65, V67, V71, V73, V75. All these stars are found as likely field stars by the membership analysis of § 3. However, while the method is very proficient in identifying the high probability cluster members as a whole, individually, the members and field stars populations can be mutually contaminated. Therefore, before labeling these variables as field stars we have taken into account other aspects of our analysis, e.g. to be considered a likely member, first, the star position of the CMD should not be obviously peculiar, as several howlers are obvious in the Fig. 5, some of which have been addressed in the above paragraphs. And second, the distance obtained from the absolute magnitude Fourier decomposition calibration and the one obtained via the P-L(*I*) relation should be similar to the general mean distance within ± 3 kpc which is about 2 sigma. Applying these considerations we are left only with the following stars V27, V41, V42, V67, V71, V73 and V75 as most likely field stars.

This paper has been typeset from a \LaTeX file prepared by the author.